

VARIANCE-INFORMED ROUNDING UNCERTAINTY ANALYSIS FOR FLOATING-POINT STATISTICAL MODELS*

SAHIL BHOLA[†] AND KARTHIK DURAISAMY[†]

Abstract. Advancements in computer hardware have made it possible to utilize low- and mixed-precision arithmetic for enhanced computational efficiency. In practical predictive modeling, however, it is vital to quantify uncertainty due to rounding along other sources like measurement, sampling, and numerical discretization. Traditional deterministic rounding uncertainty analysis (DBEA) assumes that the rounding errors are equal to the unit roundoff u . However, despite providing strong guarantees, DBEA dramatically overestimates rounding uncertainty. This work presents a novel probabilistic rounding uncertainty analysis called VIBEA. By treating rounding errors as i.i.d. random variables and leveraging concentration inequalities, VIBEA provides high-confidence estimates for rounding uncertainty by exploiting higher-order rounding error statistics. The presented framework is valid for all problem sizes n , unlike DBEA, which necessitates $nu < 1$. Further, it can account for the potential cancellation of rounding errors, resulting in rounding uncertainty estimates that grow slowly with n . We show that for $n > n_c(u)$, VIBEA produces tighter estimates for rounding uncertainty than DBEA. We also show that VIBEA improves on existing probabilistic rounding uncertainty analysis techniques for $n \geq 3$ by exploiting higher-order rounding error statistics. We conduct numerical experiments on random vector dot products, a linear system solution, and a stochastic boundary value problem. We show that quantifying rounding uncertainty along with traditional sources (numerical discretization, sampling, parameters) enables a more efficient allocation of computational resources, thereby balancing computational efficiency with predictive accuracy. This study is a step towards a comprehensive mixed-precision approach that improves model reliability and enables budgeting of computational resources in predictive modeling and decision-making.

Key words. low-precision arithmetic, floating point errors, probabilistic rounding, uncertainty quantification

1. Introduction. In recent years, low-precision arithmetic has gained significant attention in applications such as deep learning [12, 42, 24], climate modeling [35, 30, 15], solution of linear systems of equations [23, 13, 14, 2, 5], fluid dynamics [32, 37, 28], and natural sciences [31]. This is primarily motivated by the lower computational complexity, faster memory access time, a smaller energy footprint, and enhanced data parallelism offered by operating on low-precision numerical data [3, 33, 22, 2, 10, 36]. This strategy for approximate computing is becoming increasingly viable due to advancements in computer architecture (for example, Google’s TPUs and NVIDIA’s GPUs) that provide support for low- or mixed-precision computations for energy efficiency. For example, NVIDIA’s Blackwell architecture supports 4-bit floating-point representation and is estimated to deliver 1.4 exaflops on a single GPU [1].

Despite the computational advantages, operating on low-precision numerical data introduces significant rounding errors, which can accumulate through successive computations and ultimately impact the accuracy of the computation. This trade-off between computational efficiency and model reliability makes it particularly critical to quantify the uncertainty induced by rounding in conjunction with traditional sources such as measurement, sampling, and numerical discretization [38, 41, 7, 28]. Rigorously quantifying rounding uncertainty alongside traditional sources of uncertainty enables an accurate assessment of computational trade-offs and ensures model integrity where precision is balanced against efficiency.

Traditionally, the uncertainty introduced due to rounding has been studied by

*Submitted to the editors DATE.

Funding: NSF Grant FMITF-2219997 supported this research

[†]Computational Aerosciences Lab (CASLAB), Department of Aerospace Engineering, University of Michigan, Ann Arbor, MI 48109, U.S.A. (sbhola@umich.edu, kdur@umich.edu)

the deterministic treatment of rounding errors wherein rounding errors in every operation are assumed to be the unit roundoff [17, 18, 19, 34, 29, 6]. This approach produces conservative uncertainty estimates and involve the problem-size dependent constant $\gamma_n \triangleq nu/(1 - nu)$ that holds under $nu < 1$. Thus, in the regime of large problem sizes and low precision, these bounds fail to produce valid estimates for the rounding uncertainty. For example, even for the dot product of vectors of dimension 10^3 computed in single-precision (fp32), the deterministic approach overestimates the rounding uncertainty by $\mathcal{O}(10^2)$ [20].

Several studies have provided a probabilistic description for rounding errors to account for the potential cancellation and magnification of rounding errors to obtain tighter estimates of rounding uncertainty [40, 25, 16, 39, 27]. This has resulted in the heuristic that all problem-size dependent constants in estimating rounding uncertainty can be replaced by their square roots [43, 44]. Recently, pioneering work by Higham and Mary [20] provided a rigorous proof of this widely used criterion by modeling rounding errors as zero-mean independent random variables and thereby introducing a probabilistic problem-size dependent constant $\tilde{\gamma}_n \propto \sqrt{nu}$. Numerical experiments on dot products, matrix-matrix multiplication, and the solution to a dense linear system demonstrated tighter estimates for rounding uncertainty than the deterministic approach. Following [20], Higham and Mary [21] modeled numerical data as independent random variables and considered rounding errors as zero-mean random variables that are mean-independent of all previous numerical data and rounding errors. It was shown that for numerical data distributed with near zero mean, $\tilde{\gamma}_n$ can be relaxed to $\tilde{\gamma}_c \propto cu$ where c is a problem-size independent constant. However, in most practical applications (for example, the solution of linear systems and partial differential equations), numerical data cannot be assumed to be independent as it depends on a previously computed numerical value. More recently, Connolly and Higham [8] showed that tighter probabilistic estimates for rounding uncertainty can be obtained for QR factorization by modeling rounding errors as mean-independent random variables with zero means. Studies thus far have shown tighter estimates of rounding uncertainty can be obtained by exploiting the statistical effect introduced by modeling rounding errors as random variables. However, the probabilistic estimates developed have only considered first-order statistics of the rounding errors.

Building on the research of Higham and collaborators, the present work presents a novel probabilistic rounding uncertainty analysis that uses a probabilistic description for rounding errors and can exploit its higher-order statistics. We model rounding errors as an i.i.d. random variable distributed as $\mathcal{U}[-u, u]$ and utilize concentration inequalities that can exploit the mean and variance information of the rounding errors. Following a rigorous proof, we obtain rounding uncertainty estimates that have the constant $\tilde{\gamma}_n \propto \sqrt{nu}$ which holds with probability at least $\mathcal{T}(\lambda, u, n)$. In contrast to existing rounding uncertainty analysis, the proposed approach has the following advantages. First, the rounding uncertainty analysis is valid for all problem sizes, unlike the deterministic approach, which requires $nu < 1$. Second, modeling rounding errors as random variables does not discount the potential cancellation of rounding errors. Third, the proposed approach can exploit higher-order rounding error statistics, producing tighter estimates for rounding uncertainty for large problem sizes. To motivate applications in predictive modeling tasks, our rounding error analysis is cast in a systematic framework for quantifying rounding uncertainty in statistical models with other traditional sources of uncertainty, such as limited measurements, finite sampling, or numerical discretization.

The manuscript is organized as follows. In §2, rounding uncertainty due to

floating-point representation and its interpretation via backward and forward error analysis is presented. In §3, the variance-informed probabilistic rounding uncertainty analysis is presented. In §4, we derive the rounding uncertainty estimates for the dot-product and solution of a tri-diagonal system linear system using the Thomas algorithm. Numerical experiments conducted on dot-products of random vectors and a stochastic boundary value problem are presented in §5. The estimates for rounding uncertainty are then systematically compared with other sources of uncertainty, such as numerical discretization and finite sampling. Concluding remarks are presented in §6.

Notation: Scalars are denoted using lowercase letters, for example, a , vectors are denoted using bold lowercase, for example, \mathbf{a} , and matrices are denoted using bold uppercase, for example, \mathbf{A} . Elements of vectors and matrices are denoted using subscripts, that is, $\mathbf{A}_{i,j}$ would be the element in the i^{th} row and j^{th} column. Inequalities established for vectors and matrices hold componentwise, that is, $|\mathbf{A}| \leq |\mathbf{B}|$ means that $|\mathbf{A}_{i,j}| \leq |\mathbf{B}_{i,j}| \forall i, j$. Perturbation to a vector or a matrix is defined componentwise, that is, $\mathbf{A} + \Delta\mathbf{A}$ wherein $\Delta\mathbf{A}$ is the perturbation would mean $\mathbf{A}_{i,j} + \Delta\mathbf{A}_{i,j} \forall i, j$.

2. Rounding Errors in Floating-Point Statistical Models. The floating-point number system $\mathbb{F} \subset \mathbb{R}$ consists of numbers with the form

$$(2.1) \quad y \triangleq \pm d_0.d_1d_2 \cdots d_{p-1} \times \beta^e,$$

where p is the *precision*, β is the *base*, and $e \in [e_{min}, e_{max}]$ is the *exponent*. Given the tuple $t^* \triangleq (p, \beta, e_{min}, e_{max})$, a finite and unique set of representable numbers can be obtained that defines a floating-point system. Representing $z \in \mathbb{R}$ in a floating-point number system characterized by t^* thus requires a projection operation $fl : \mathbb{R} \rightarrow \mathbb{F}$ such that $fl(z) \in \mathbb{F}$ is a representable number. This projection operation to a representable number is called *representation-rounding*. A similar rounding operation occurs when finite-precision arithmetic operations are performed. For $a, b \in \mathbb{F}$, computing $(a \text{ op } b)$ where $op \in \{+, -, \times, /\}$ in the prescribed precision requires a projection to a representable number $fl(a \text{ op } b) \in \mathbb{F}$. This projection operation associated with finite-precision arithmetic is called *operation-rounding*. The loss of information due to representation- or operation-rounding introduces rounding errors that grow during successive computations, thus introducing rounding uncertainty in the computational model. As a result, computing any function $\varphi : \mathbb{R}^{n_{in}} \rightarrow \mathbb{R}^{n_{out}}$ in finite precision produces an approximation $\hat{\mathbf{y}}$ of $\mathbf{y} = \varphi(\mathbf{x})$, which is the true output of an approximate function $\hat{\varphi}$ as illustrated in Figure 1. To measure the quality of approximation $\hat{\mathbf{y}}$, *forward errors* can be defined, which are the absolute or relative errors described in the output space. Since the true output \mathbf{y} is typically unknown, forward error bounds can be developed (a process called forward error analysis) to estimate the uncertainty introduced due to rounding. Alternatively, the uncertainty introduced due to rounding can be interpreted as a consequence of perturbations in the input space that propagates through the true function φ . To this end, an input perturbation $\Delta\mathbf{x}$ can be defined to find the set of inputs that solves the actual problem, that is, $\varphi(\mathbf{x} + \Delta\mathbf{x}) = \hat{\varphi}(\mathbf{x})$. Since $\Delta\mathbf{x}$ can be non-unique, the smallest relative perturbation to the input space called the *backward error* can be defined. This can be obtained as the solution to an optimization problem

$$(2.2) \quad \epsilon_{bwd} \triangleq \min\{\epsilon \geq 0 : \hat{\mathbf{y}} = \varphi(\mathbf{x} + \Delta\mathbf{x}), |\Delta\mathbf{x}| \leq \epsilon|\mathbf{x}|\}.$$

In practical applications, bounding backward error can be advantageous as it can be (a) directly compared with uncertainties in \mathbf{x} and (b) used to derive forward error

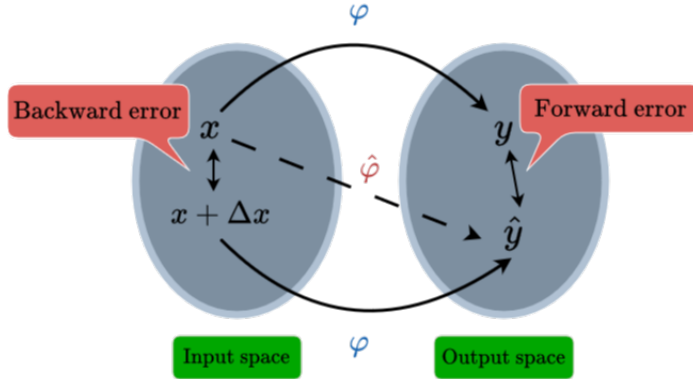


FIG. 1. Schematic of backward and forward errors. Solid line: exact; dashed line: computed.

bounds. These advantages motivate using a backward error analysis approach to estimate rounding uncertainty in this work.

2.1. Model for Rounding Error. Backward error implicitly depends upon the rounding operation. Therefore, we need a model for the underlying rounding operation to obtain backward error estimates and develop useful error bounds.

For IEEE standard [26], representation-rounding can be modeled as

$$(2.3) \quad fl(z) \triangleq z(1 + \delta_r)^\rho; \quad z \in \mathbb{R}, \rho = \pm 1, |\delta_r| \leq u,$$

where δ_r is the *rounding error due to representation* [19]. Here, $\rho = 1$ for the standard computation model and $\rho = -1$ for the alternate computational model. Similarly, the classical IEEE arithmetic model can be used to model operation-rounding as

$$(2.4) \quad fl(a \text{ op } b) \triangleq (a \text{ op } b)(1 + \delta_{op})^\rho; \quad a, b \in \mathbb{F}, |\delta_{op}| \leq u, \text{ op} \in \{+, -, \times, /\},$$

where δ_{op} is the *rounding error due to operation*. The motivation for using (2.4) is that the computed value of $a \text{ op } b$ is as good as the rounded true value. However, it should be noted that the classical arithmetic model does not capture all rounding artifacts. For example, $\delta_{op} = 0$ is not enforced for $(a \text{ op } b) \in \mathbb{F}$ and $\rho = 1$.

In this work, rounding errors are modeled as random variables using the following model.

MODEL 2.1 (Rounding error model). *Rounding error due to finite-precision representation or arithmetic is an i.i.d. random variable with density $\mathcal{U}[-u, u]$.*

Figure 2 illustrates the empirical cumulative distribution function (CDF) of the rounding error due to representation. For $z \in \mathcal{U}[2^k, 2^{k+1}] \forall k \in \mathbb{I}$, a similar CDF is obtained as a consequence of uniform spacing between representable numbers within the interval $[\beta^k, \beta^{k+1}]$ [19]. Furthermore, Model 2.1 results in a larger rounding error with a higher probability. This overestimation of error is critical because any backward error bounds based on Model 2.1 should not underestimate the value to be bounded. Similar observations can be made for rounding errors due to operations; Figures 3 and 4 show the empirical CDF for finite-precision addition and multiplication operations, respectively. However, Model 2.1 is not always realistic. For example, the rounding error must be zero when adding, subtracting, or multiplying integer values.

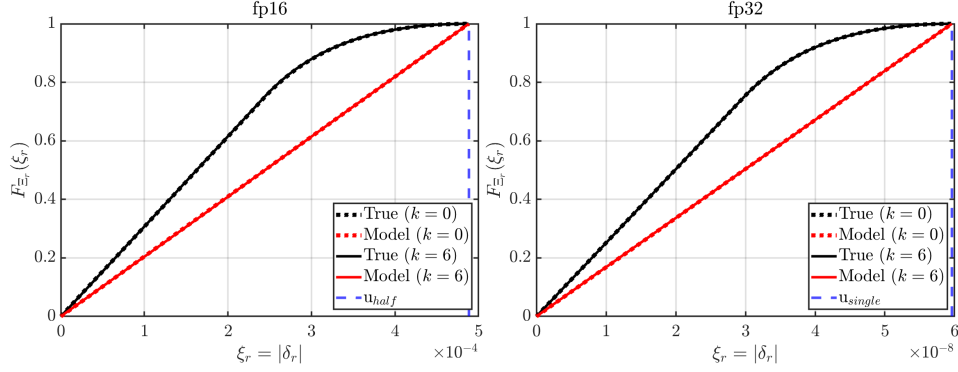


FIG. 2. Empirical CDF of the rounding error due to representation of $z \sim \mathcal{U}[2^k, 2^{k+1}]$ in half-precision (left) and single-precision (right) using the standard computational model. Double-precision computation is considered the exact result.

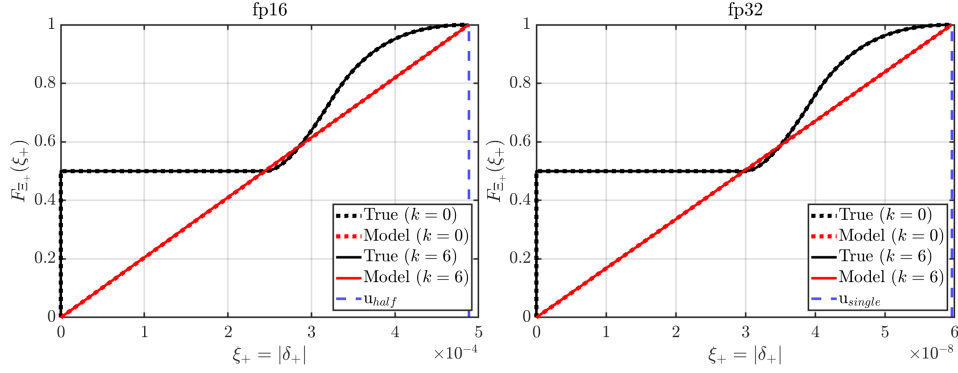


FIG. 3. Empirical CDF of rounding error due to addition operation $fl(a+b)$ with $a, b \in \mathbb{F}$ and $a, b \sim \mathcal{U}[2^k, 2^{k+1}]$ in half-precision (left) and single-precision (right) using the standard computational model. Double-precision computation is considered the exact result.

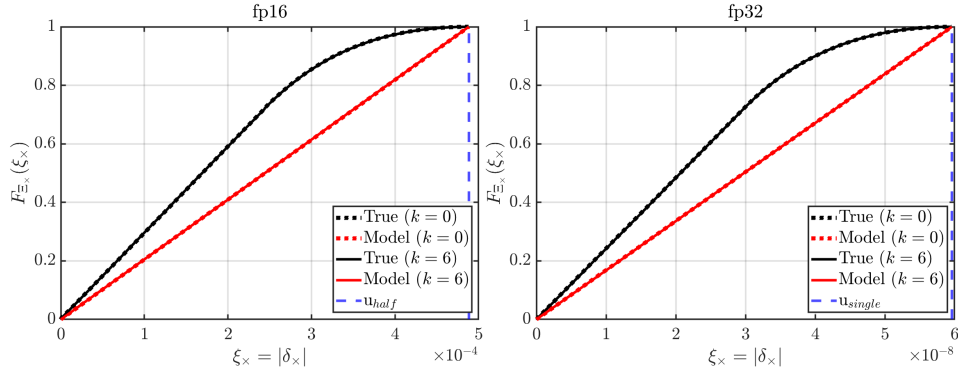


FIG. 4. Empirical CDF of rounding error due to multiplication operation $fl(a \times b)$ with $a, b \in \mathbb{F}$ and $a, b \sim \mathcal{U}[2^k, 2^{k+1}]$ in single-precision (left) and half-precision (right) using the standard computational model. Double-precision computation is considered the exact result.

Nevertheless, the motivation for using [Model 2.1](#) is to obtain reasonable estimates for rounding uncertainty on average.

3. Bounds for the Product of Rounding Errors. Performing backward error analysis on numerical algorithms results in the product of terms in the form of $(1 + \delta_i)^{\rho_i}$, where δ_i denotes the rounding error due to representation/operation and $\rho_i = \pm 1$ [19]. These terms arise due to the model introduced for rounding operations. For example, consider $y = \sum_{i=1}^3 a_i b_i$ where $a_i, b_i \in \mathbb{R}$. Using (2.3) and (2.4), the computed approximation to y is given as $\hat{y} = \sum_{i=1}^3 a_i b_i (1 + \eta_i)(1 + \zeta_i)(1 + \xi_i) \prod_{j=\max(2,i)}^3 (1 + \kappa_j)$ assuming recursive summation from left to right. Here, $\eta_i, \zeta_i, \xi_i, \kappa_j$ are the rounding errors, and it is assumed that addition to zero does not introduce any rounding error. In backward error analysis, a bound for the product $\prod_{i=1}^n (1 + \delta_i)^{\rho_i}$ is sought to obtain a perturbed system.

Deterministic Backward Error Analysis (DBEA). In the traditional backward analysis, the following lemma [19, Lemma 3.1] is used to bound the distance between 1 and the product $\prod_{i=1}^n (1 + \delta_i)^{\rho_i}$.

LEMMA 3.1 (Deterministic rounding error bound). *If $|\delta_i| \leq u$ and $\rho_i = \pm 1$ for $i = 1, \dots, n$, and $nu < 1$, then*

$$\prod_{i=1}^n (1 + \delta_i)^{\rho_i} \triangleq 1 + \theta_n,$$

with $|\theta_n| \leq \gamma_n(u, n) = \frac{nu}{1-nu}$.

However, this analysis results in conservative estimates for the backward error as it only uses $|\delta_i| \leq u$ and cannot possibly exploit the cancellation of rounding errors [20, 9].

Mean-informed Backward Error Analysis (MIBEA). Modeling the rounding errors as random variables has resulted in the heuristic: all constants in the rounding uncertainty analysis that depend on the problem size can be replaced by their square root. Higham and Mary [20] presented a rigorous proof for this criteria and showed that by modeling rounding errors as zero-mean independent random variables, the problem-size dependent constant γ_n in [Lemma 3.1](#) can be replaced with

$$(3.1) \quad \tilde{\gamma}_n(\lambda, u, n) \triangleq \exp\left(\lambda\sqrt{nu} + \frac{nu^2}{1-u}\right) - 1 \leq \lambda\sqrt{nu} + \mathcal{O}(u^2),$$

such that $|\theta_n| \leq \tilde{\gamma}_n$ with probability at least

$$(3.2) \quad p_h(\lambda, u) \triangleq 1 - 2 \exp\left(\frac{-\lambda(1-u)^2}{2}\right).$$

However, the obtained probabilistic bounds utilize Hoeffding's concentration inequality ([Lemma 3.2](#)) and thus ignore higher-order rounding error statistics.

LEMMA 3.2 (Hoeffding's Inequality). *Let Z_1, \dots, Z_n be n independent random variables such that $p(|Z_i| \leq c_i) = 1 \forall i$. Then the random variable $S_n \triangleq \sum_{i=1}^n Z_i$ satisfies*

$$p(|S_n - \mathbb{E}[S_n]| \geq t) \leq 2 \exp\left(\frac{-t^2}{2 \sum_{i=1}^n c_i^2}\right),$$

$\forall t > 0$.

Variance-informed Backward Error Analysis (VIBEA). We will now introduce a rounding uncertainty analysis that incorporates higher-order statistics. Similar to [20], the sum of random variables $\sum_{i=1}^n \rho_i \log(1 + \delta_i)$ are bounded by means of a concentration inequality. Specifically, Bernstein's concentration inequality is used to bound the probability that random variable $S_n \triangleq \sum_{i=1}^n Z_i$ deviates from $\mathbb{E}[S_n]$ by a given quantity for a bounded random variable Z_i [4].

LEMMA 3.3 (Bernstein's Inequality). *Let Z_1, \dots, Z_n be n independent random variables such that $p(|Z_i| \leq c) = 1$. Then the random variable $S_n \triangleq \sum_{i=1}^n Z_i$ satisfies*

$$p(|S_n - \mathbb{E}[S_n]| \geq t) \leq 2 \exp\left(\frac{-t^2}{2(\sigma^2 + \frac{ct}{3})}\right),$$

$\forall t > 0$, where $\sigma^2 \triangleq \sum_{i=1}^n \text{Var}[Z_i]$.

We can now derive the variance-informed probabilistic backward error bounds using Bernstein's concentration inequality.

THEOREM 3.4 (Variance-informed probabilistic error bounds). *Let $\delta_1, \dots, \delta_n$ represent n i.i.d. random variables distributed uniformly as $\mathcal{U}[-u, u]$ where $u \leq 1$. Then for $\lambda \geq 0$*

$$\prod_{i=1}^n (1 + \delta_i)^{\rho_i} = 1 + \theta_n,$$

hold such that $|\theta_n| \leq \tilde{\gamma}_n(\lambda, u)$ with probability at least

$$p_b(\lambda, u, n) \triangleq 1 - 2 \exp\left(\frac{-\lambda^2 n u^2}{2(\sigma^2 + \frac{\lambda \sqrt{n} u^2}{3(1-u)})}\right),$$

where

$$\sigma^2 = n \left(\frac{4u^2 + \kappa(\log(1-u))^2 - 2 \log(1-u) \log(1+u) + \log(1+u)^2}{4u^2} \right),$$

with $\kappa = (-1 + u^2)$.

Proof. Define $\log \phi \triangleq \sum_{i=1}^n \rho_i \log(1 + \delta_i)$ as the sum of n i.i.d. random variables. For $|\delta_i| \leq u \leq 1$, we can bound $\log(1 + \delta_i)$ using Taylor series expansion as

$$\begin{aligned} \delta_i - \sum_{k=2}^{\infty} |\delta_i|^k &\leq \log(1 + \delta_i) \leq \delta_i + \sum_{k=2}^{\infty} |\delta_i|^k, \\ \delta_i - \frac{\delta_i^2}{1 - |\delta_i|} &\leq \log(1 + \delta_i) \leq \delta_i + \frac{\delta_i^2}{1 - |\delta_i|}, \end{aligned}$$

such that $|\rho_i \log(1 + \delta_i)| \leq \frac{u}{1-u}$. Applying **Lemma 3.3** with $Z_i = \rho_i \log(1 + \delta_i)$ and $c = \frac{u}{1-u}$

$$p(|\log \phi - \mathbb{E}[\log \phi]| \geq t) \leq 2 \exp\left(\frac{-t^2}{2(\sigma^2 + \frac{ut}{3(1-u)})}\right).$$

Since $\mathbb{E}[\delta_i] = 0$, we can obtain $\mathbb{E}[\log \phi] \leq \frac{nu^2}{1-u}$, such that

$$|\log \phi - \mathbb{E}[\log \phi]| \geq |\log \phi| - |\mathbb{E}[\log \phi]| \geq |\log \phi| - \frac{nu^2}{1-u}.$$

This gives

$$p(|\log \phi| - \frac{nu^2}{1-u} \geq t) \leq p(|\log \phi - \mathbb{E}[\log \phi]| \geq t) \leq 2 \exp\left(\frac{-t^2}{2(\sigma^2 + \frac{ut}{3(1-u)})}\right),$$

where for [Model 2.1](#)

$$\sigma^2 = n \left(\frac{4u^2 + \kappa(\log(1-u))^2 - 2\log(1-u)\log(1+u) + \log(1+u)^2}{4u^2} \right),$$

where $\kappa \triangleq (-1 + u^2)$. Similar to [\[20\]](#), we can assume the functional-form $t(\lambda, n, u) = \lambda\sqrt{nu}$, which gives

$$p(|\log \phi| \leq \lambda\sqrt{nu} + \frac{nu}{1-u}) \geq 1 - 2 \exp\left(\frac{-\lambda^2 nu^2}{2(\sigma^2 + \frac{\lambda\sqrt{nu^2}}{3(1-u)})}\right) = p_b(\lambda, u, n),$$

such that

$$|\phi - 1| \leq \exp(\lambda\sqrt{nu} + \frac{nu}{1-u}) - 1 \leq \lambda\sqrt{nu} + \mathcal{O}(u^2),$$

holds with probability of at least p_b for $0 \leq \lambda\sqrt{nu} + \frac{nu}{1-u} < 1$. \square

The constant term $\tilde{\gamma}_n$ is similar to that obtained via MIBEA; however, the probability lower bound p_b contains higher-order statistics of the rounding errors. We can then define a critical λ -parameter as $\lambda_c^b(\alpha, u, n) = \min\{\lambda \geq 0 : |p_b - \alpha|\}$, and $\lambda_c^h(\alpha, u) = \min\{\lambda \geq 0 : |p_h - \alpha|\}$ to compare MIBEA with the presented framework. Here, α is the minimum required confidence for the rounding error bounds to be satisfied. As shown in [Figure 5](#), $\lambda_c^b < \lambda_c^h$ for $n \geq 3$ (for both single- and half-precision) and therefore would result in tighter probabilistic bounds ($\tilde{\gamma}_n \propto \lambda$) for the same required confidence in error bounds. Further, for the VIBEA to result in tighter bounds than those obtained using DBEA, the condition $\lambda\sqrt{n} \leq n/(1-nu)$ must be true. Thus, a critical problem size $n_c(\lambda, u)$ can be defined for which high-confidence probabilistic bounds that are tighter than those obtained via the deterministic approach can be obtained. For $\lambda \in \{\lambda_c^h, \lambda_c^b\}$, the critical problem sizes are tabulated in [Table 1](#). As noticed, $n_c(\lambda_c^b) < n_c(\lambda_c^h)$ for all the required confidence levels and precision, and for $n > 50$ VIBEA always produces tighter estimates of rounding uncertainty compared to DBEA.

4. Adaptation in Numerical Linear Algebra. In this section, variance-informed backward error analysis is conducted for (a) the dot product of vectors and (b) solving a tri-diagonal linear system. While the dot product is a fundamental operation in various numerical algorithms, banded matrices are widely observed in statistical models in applications such as fluid or structural dynamics and control theory. Since in most practical applications, we are interested in accumulated rounding error *once the statistical model is expressed in finite-precision*, here, we consider rounding error accumulation without any representation-rounding.

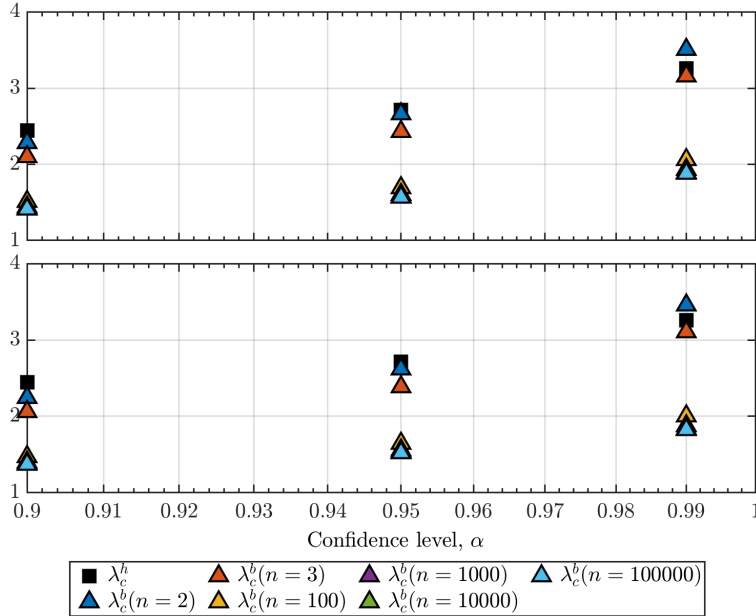

 FIG. 5. Critical λ -parameter vs. confidence level α for fp16 (top) and fp32 (bottom) arithmetic.

 TABLE 1
 Critical problem size for various confidence levels.

α	$n_c(\lambda_c^h)$		$n_c(\lambda_c^b)$	
	fp16	fp32	fp16	fp32
0.9	7	7	5	4
0.95	8	8	5	5
0.99	11	11	8	7
1.0	72	77	50	50

4.1. Dot Product. Using [Theorem 3.4](#), we now develop variance-informed probabilistic backward error bounds for dot products.

THEOREM 4.1 (Dot product). *Let $y = \mathbf{a}^T \mathbf{b}$, where $\mathbf{a}, \mathbf{b} \in \mathbb{F}^n$ characterized by the tuple t^* . Under the [Model 2.1](#), the computed dot-product \hat{y} satisfies*

$$\hat{y} = (\mathbf{a} + \Delta \mathbf{a})^T \mathbf{b} = \mathbf{a}^T (\mathbf{b} + \Delta \mathbf{b}),$$

where $|\Delta \mathbf{a}| \leq \tilde{\gamma}_n |\mathbf{a}|$ and $|\Delta \mathbf{b}| \leq \tilde{\gamma}_n |\mathbf{b}|$ holds with a probability at least

$$\mathcal{T}_D^b(\lambda, u, n) \triangleq 1 - \sum_{i=1}^n (1 - p_b(\lambda, u, n - \max(2, i) + 2)).$$

Proof. Assume that the dot product is computed via the recursive relation $s_i = s_{i-1} + a_i b_i$ where $s_0 = 0$, such that the true dot product $y = s_n$. The computed

intermediate sum \hat{s}_i can then be represented as

$$\hat{s}_i = (\hat{s}_{i-1} + a_i b_i (1 + \eta_i))(1 + \zeta_i); \quad |\eta_i|, |\zeta_i| \leq u,$$

where η_i and ζ_i are the rounding error due to multiplication and addition, respectively. Here, $\zeta_1 = 0$ since addition to $s_0 = \hat{s}_0 = 0$ does not introduce any rounding error. Therefore, the computed dot product \hat{y} is

$$\begin{aligned} \hat{y} &= \sum_{i=1}^n a_i b_i (1 + \eta_i) \prod_{j=\max(2,i)}^n (1 + \zeta_j), \\ &= \sum_{i=1}^n a_i b_i (1 + \theta_{n-\max(2,i)+2}) = \sum_{i=1}^n (a_i + \Delta a_i) b_i = \sum_{i=1}^n a_i (b_i + \Delta b_i), \end{aligned}$$

where $\Delta a_i \triangleq a_i \theta_{i'}$ and $\Delta b_i \triangleq b_i \theta_{i'}$ with $i' \triangleq n - \max(2, i) + 2$. Thus,

$$\begin{aligned} |\Delta a_i| &\leq |a_i| |\theta_{i'}|, \\ |\Delta b_i| &\leq |b_i| |\theta_{i'}|, \end{aligned}$$

with $|\theta_{i'}| \leq \tilde{\gamma}_{i'} \leq \tilde{\gamma}_n$ with probability at least $p_b(\lambda, u, i')$. Thus, the bound $|\theta_{i'}| \leq \tilde{\gamma}_n$ fails with probability at most $1 - p_b(\lambda, u, i')$. Therefore, from the principle of inclusion-exclusion of probabilities we can obtain that for all $i = 1, \dots, n$ the corresponding bounds fail with probability at most $\sum_{i=1}^n (1 - p_b(\lambda, u, i'))$. This gives the probability of all bounds being satisfied at least

$$\mathcal{T}_D^b(\lambda, u, n) = 1 - \sum_{i=1}^n (1 - p_b(\lambda, u, i')). \quad \square$$

A similar analysis can be conducted following DBEA, wherein the computed dot-product \hat{y} satisfies $\hat{y} = (\mathbf{a} + \Delta \mathbf{a})^T \mathbf{b} = \mathbf{a}^T (\mathbf{b} + \Delta \mathbf{b})$ with $|\Delta \mathbf{a}| \leq \gamma_n |\mathbf{a}|$ and $|\Delta \mathbf{b}| \leq \gamma_n |\mathbf{b}|$. Higham and Mary [20] obtained bounds similar to [Theorem 4.1](#), however, with a probability lower bound of

$$(4.1) \quad \mathcal{T}_D^h(\lambda, u, n) = 1 - n(1 - p_h).$$

Using [Theorem 4.1](#), the variance-informed relative forward error bound is then given as

$$(4.2) \quad \frac{|\hat{y} - y|}{|y|} \leq \tilde{\gamma}_n \mathcal{C}_D; \quad \mathcal{C}_D \triangleq \frac{|\mathbf{a}^T| |\mathbf{b}|}{|\mathbf{a}^T \mathbf{b}|},$$

which holds with probability at least \mathcal{T}_D^b . Similarly, for DBEA, the relative forward error bound is $\gamma_n \mathcal{C}_D$, and for MIBEA, it is given as $\tilde{\gamma}_n \mathcal{C}_D$, which holds with probability at least \mathcal{T}_D^h .

4.2. Thomas Algorithm. Thomas algorithm is widely used to compute the solution of a tri-diagonal system $\mathbf{A} \mathbf{x} = \mathbf{b}$. Broadly, it consists of three steps

1. Compute LU-factorization of \mathbf{A} as $\mathbf{L} \mathbf{U} = \mathbf{A}$.
2. Perform forward substitution to solve the system $\mathbf{L} \mathbf{y} = \mathbf{b}$.
3. Perform backward substitution to solve the system $\mathbf{U} \mathbf{x} = \mathbf{y}$.

Computing the solution of the system in finite precision is therefore associated with rounding errors in all three steps. Thus, to determine the backward error bounds on \mathbf{A} we must first individually determine backward error bounds for each of the outlined steps. First, consider the LU-factorization for which the variance-informed backward error bound is given in [Lemma 4.2](#).

LEMMA 4.2 (LU decomposition of tri-diagonal system). *Let $\mathbf{A} = \mathbf{LU}$ be the LU-factorization of a tri-diagonal matrix $\mathbf{A} \in \mathbb{F}^{n \times n}$ characterized by the tuple t^* . Then, under [Model 2.1](#) the computed factorization $\hat{\mathbf{L}} \in \mathbb{F}^{n \times n}$ and $\hat{\mathbf{U}} \in \mathbb{F}^{n \times n}$ via Doolittle's method satisfies*

$$\hat{\mathbf{L}}\hat{\mathbf{U}} = \mathbf{A} + \Delta\mathbf{A},$$

such that $|\Delta\mathbf{A}| \leq \tilde{\gamma}_1 |\hat{\mathbf{L}}| |\hat{\mathbf{U}}|$ holds with a probability at least

$$\mathcal{T}_{LU}^b(\lambda, \mathbf{u}, n) \triangleq 1 - (n-1)(1 - \mathcal{Q}_{LU}^b),$$

where $\mathcal{Q}_{LU}^b \triangleq 1 - 3(1 - p_b(\lambda, \mathbf{u}, 1))$.

Proof. Let $\mathbf{A} \in \mathbb{F}^{n \times n}$ be a tri-diagonal matrix with non-zero elements

$$\mathbf{A}_{i,j} = \begin{cases} \alpha_i & \text{for } j = i-1 \text{ and } i = 2, \dots, n, \\ \beta_i & \text{for } j = i \text{ and } i = 1, \dots, n, \\ \nu_i & \text{for } j = i+1 \text{ and } i = 1, \dots, n-1, \end{cases}$$

with $\alpha_i, \beta_i, \nu_i \in \mathbb{F}$. Let $\mathbf{A} = \mathbf{LU}$ be the LU-factorization where the non-zero elements of the factorization are given as

$$\mathbf{L}_{i,j} = \begin{cases} l_i & \text{for } j = i-1 \text{ and } i = 2, \dots, n, \\ 1 & \text{for } j = i \text{ and } i = 1, \dots, n, \end{cases}$$

$$\mathbf{U}_{i,j} = \begin{cases} u_i & \text{for } j = i \text{ and } i = 1, \dots, n, \\ \nu_i & \text{for } j = i+1 \text{ and } i = 1, \dots, n-1. \end{cases}$$

The non-zero elements can be obtained using a recurrence relation via Doolittle's method as

$$\left. \begin{array}{l} l_i = \alpha_i / u_{i-1}, \\ u_i = \beta_i - l_i \nu_{i-1}, \end{array} \right\} \quad \text{for } i = 2, \dots, n,$$

with $u_1 = \beta_1$, such that for any $i = 2, \dots, n$ the computed elements of the factorization are

$$\hat{l}_i = \alpha_i / \hat{u}_{i-1} (1 + \eta_i); \quad |\eta_i| \leq \mathbf{u},$$

$$\hat{u}_i = (\beta_i - \hat{l}_i \nu_{i-1} (1 + \zeta_i)) / (1 + \xi_i); \quad |\zeta_i|, |\xi_i| \leq \mathbf{u}.$$

Using [Theorem 3.4](#)

$$\hat{l}_i \hat{u}_{i-1} + \theta_1 \hat{l}_i \hat{u}_{i-1} = \alpha_i,$$

$$\hat{u}_i + \hat{l}_i \nu_{i-1} + \theta'_1 \hat{u}_i + \theta''_1 \hat{l}_i \nu_{i-1} = \beta_i,$$

where $|\theta_1|, |\theta'_1|, |\theta''_1| \leq \tilde{\gamma}_1$ is satisfied with probability at least $p_b(\lambda, u, 1)$. Thus, via the principle of inclusion-exclusion, for any i all the bounds are satisfied with probability at least $\mathcal{Q}_{LU}^b = 1 - 3(1 - p_b(\lambda, u, 1))$. In matrix notation, the computed factorization can then be expressed as

$$\hat{\mathbf{L}}\hat{\mathbf{U}} = \mathbf{A} + \Delta\mathbf{A},$$

where $|\Delta\mathbf{A}| \leq \tilde{\gamma}_1|\hat{\mathbf{L}}||\hat{\mathbf{U}}|$, such that all the bounds are satisfied for $i = 2, \dots, n$ with probability at least \square

$$\mathcal{T}_{LU}^b(\lambda, u, n) = 1 - (n-1)(1 - \mathcal{Q}_{LU}^b).$$

MIBEAs results in similar backward error bounds for LU-factorization as [Lemma 4.2](#), however, the probability lower bound is given as $\mathcal{T}_{LU}^h(\lambda, u, n) \triangleq 1 - (n-1)(1 - \mathcal{Q}_{LU}^h)$ where $\mathcal{Q}_{LU}^h \triangleq 1 - 3(1 - p_h)$.

Next, [Lemma 4.3](#) outlines the variance-informed backward error bounds for the forward substitution.

LEMMA 4.3 (Forward substitution in Thomas algorithm). *Let $\mathbf{L}\mathbf{y} = \mathbf{b}$ be a tri-diagonal system where $\mathbf{L} \in \mathbb{F}^{n \times n}$ characterized by the tuple t^* is the lower-triangular matrix obtained from the LU-factorization of a tri-diagonal matrix $\mathbf{A} \in \mathbb{F}^{n \times n}$. Then, under [Model 2.1](#) the computed solution $\hat{\mathbf{y}}$ via forward substitution satisfies*

$$(\mathbf{L} + \Delta\mathbf{L})\hat{\mathbf{y}} = \mathbf{b},$$

such that $|\Delta\mathbf{L}| \leq \tilde{\gamma}_1|\Delta\mathbf{L}|$ holds with a probability at least

$$\mathcal{T}_{FS}^b(\lambda, u, n) \triangleq 1 - (n-1)(1 - \mathcal{Q}_{FS}^b),$$

where $\mathcal{Q}_{FS}^b \triangleq 1 - 2(1 - p_b(\lambda, u, 1))$.

Proof. Let $\mathbf{L}\mathbf{y} = \mathbf{b}$ be a triangular system where \mathbf{L} is the lower-triangular matrix obtained from the LU-factorization of a tri-diagonal matrix via Dolittle's decomposition. The non-zero elements of \mathbf{L} are given as

$$\mathbf{L}_{i,j} = \begin{cases} l_i & \text{for } j = i-1 \text{ and } i = 2, \dots, n, \\ 1 & \text{for } j = i \text{ and } i = 1, \dots, n. \end{cases}$$

The system can then be solved via forward substitution as

$$y_i = \begin{cases} b_i & \text{for } i = 1, \\ b_i - l_i y_{i-1} & \text{for } i = 2, \dots, n, \end{cases}$$

such that the computed solution is given as

$$\hat{y}_i = \begin{cases} b_i & \text{for } i = 1, \\ \frac{b_i - l_i \hat{y}_{i-1} (1 + \eta_i)}{(1 + \zeta_i)} & \text{for } i = 2, \dots, n. \end{cases}$$

Using [Theorem 3.4](#) \square

$$\hat{y}_i + l_i \hat{y}_{i-1} + \theta_1 \hat{y}_i + \theta'_1 l_i \hat{y}_{i-1} = b_i,$$

where $|\theta_1|, |\theta'_1| \leq \tilde{\gamma}_1$ with probability at least $p_b(\lambda, u, 1)$. Thus, for any given i all the bounds are satisfied with probability at least $\mathcal{Q}_{FS}^b = 1 - 2(1 - p_b(\lambda, u, 1))$. In matrix notation, the computed solution can then be represented as

$$(\mathbf{L} + \Delta\mathbf{L})\hat{\mathbf{y}} = \mathbf{b},$$

where $|\Delta\mathbf{L}| \leq \tilde{\gamma}_1|\mathbf{L}|$, such that all the bounds for $i = 2, \dots, n$ are satisfied with probability at least

$$\mathcal{T}_{FS}^b(\lambda, u, n) = 1 - (n-1)(1 - \mathcal{Q}_{FS}^b).$$

Performing MIBEA results in similar backward error bounds for forward substitution as [Lemma 4.3](#), however, the probability lower bound is given as $\mathcal{T}_{FS}^h(\lambda, u, n) \triangleq 1 - (n-1)(1 - \mathcal{Q}_{FS}^h)$ where $\mathcal{Q}_{FS}^h \triangleq 1 - 2(1 - p_h)$.

Lastly, [Lemma 4.4](#) gives the variance-informed backward error bounds for the backward substitution.

LEMMA 4.4 (Backward substitution in Thomas algorithm). *Let $\mathbf{U}\mathbf{x} = \mathbf{y}$ be a tri-diagonal system where $\mathbf{U} \in \mathbb{F}^{n \times n}$ characterized by the tuple t^* is the upper-triangular matrix obtained from the LU-factorization of a tri-diagonal matrix $\mathbf{A} \in \mathbb{F}^{n \times n}$. Then, for [Model 2.1](#) the computed solution $\hat{\mathbf{x}}$ via backward substitution satisfies*

$$(\mathbf{U} + \Delta\mathbf{U})\hat{\mathbf{x}} = \mathbf{y},$$

such that $|\Delta\mathbf{U}| \leq \tilde{\gamma}_2|\mathbf{U}|$ holds with a probability at least

$$\mathcal{T}_{BS}^b(\lambda, u, n) \triangleq 1 - [(n-1)(1 - \mathcal{Q}_{BS}^b) + (1 - \mathcal{Q}_{BSN}^b)],$$

where $\mathcal{Q}_{BS}^b \triangleq 1 - [(1 - p_b(\lambda, u, 2)) + (1 - p_b(\lambda, u, 1))]$ and $\mathcal{Q}_{BSN}^b = 1 - (1 - p_b(\lambda, u, 1))$.

Proof. Let $\mathbf{U}\mathbf{x} = \mathbf{y}$ be a triangular system where \mathbf{U} is the upper triangular matrix obtained from the LU-factorization of a tri-diagonal matrix via Dolittle's decomposition. The non-zero elements of \mathbf{U} are given as

$$\mathbf{U}_{i,j} = \begin{cases} u_i & \text{for } j = i \text{ and } i = 1, \dots, n, \\ \nu_i & \text{for } j = i + 1 \text{ and } i = 1, \dots, n-1. \end{cases}$$

The system can then be solved via backward substitution as

$$x_i = \begin{cases} y_n & \text{for } i = n, \\ \frac{y_i - \nu_i x_{i+1}}{u_i} & \text{for } i = n-1, \dots, 1, \end{cases}$$

such that the computed solution is given as

$$\hat{x}_i = \begin{cases} \frac{y_n}{u_n(1+\eta_i)} & \text{for } i = n, \\ \frac{y_i - \nu_i \hat{x}_{i+1}(1+\zeta_i)}{u_i(1+\xi_i)(1+\chi_i)} & \text{for } i = n-1, \dots, 1, \end{cases}$$

where $|\eta_i|, |\zeta_i|, |\xi_i|, |\chi_i| \leq u$. Using [Theorem 3.4](#)

$$\begin{aligned} \hat{x}_n u_n + \theta_1 \hat{x}_n u_n &= y_n, \\ u_i \hat{x}_i + \nu_i \hat{x}_{i+1} + \theta_2 u_i \hat{x}_i + \theta'_1 \nu_i \hat{x}_{i+1} &= y_i; \quad \text{for } i = n-1, \dots, 1, \end{aligned}$$

where $|\theta_1|, |\theta'_1| \leq \tilde{\gamma}_1 \leq \tilde{\gamma}_2$ with probability at least $p_b(\lambda, u, 1)$. Similarly, $|\theta_2| \leq \tilde{\gamma}_2$ with probability at least $p_b(\lambda, u, 2)$. Thus, for any $i = n-1, \dots, 1$ the bounds are satisfied with probability at least $\mathcal{Q}_{BS}^b = 1 - [(1 - p_b(\lambda, u, 2)) + (1 - p_b(\lambda, u, 1))]$, and for $i = n$ the bounds are satisfied with probability at least $\mathcal{Q}_{BSN}^b = 1 - (1 - p_b(\lambda, u, 1))$. In matrix notation, the computed solution can then be represented as

$$(\mathbf{U} + \Delta\mathbf{U})\hat{\mathbf{x}} = \mathbf{y},$$

where $|\Delta\mathbf{U}| \leq \tilde{\gamma}_2|\mathbf{U}|$, such that all the bounds for $i = 1, \dots, n$ are satisfied with probability at least \square

$$\mathcal{T}_{BS}^b(\lambda, u, n) = 1 - [(n-1)(1 - \mathcal{Q}_{BS}^b) + (1 - \mathcal{Q}_{BSN}^b)].$$

Performing MIBEAs results in similar backward error bounds for backward substitution as [Lemma 4.4](#), however, the probability lower bound is given as $\mathcal{T}_{BS}^h(\lambda, u, n) \triangleq 1 - [(n-1)(1 - \mathcal{Q}_{BS}^h) + (1 - p_h)]$ where $\mathcal{Q}_{BS}^h \triangleq 1 - 2(1 - p_h)$.

Now, using [Lemmas 4.2 to 4.4](#) we can derive variance-informed backward error bounds for solving a tri-diagonal system of equations.

THEOREM 4.5. *Let $\mathbf{Ax} = \mathbf{b}$ be a tri-diagonal system with $\mathbf{A} \in \mathbb{F}^{n \times n}$, $\mathbf{x} \in \mathbb{F}^n$ and $\mathbf{b} \in \mathbb{F}^n$ are characterized by the tuple t^* . Assume that $\hat{\mathbf{L}}$ and $\hat{\mathbf{U}}$ are the computed LU-factorization of the matrix \mathbf{A} via Doolittle's decomposition. Then, under [Model 2.1](#) the computed solution $\hat{\mathbf{x}}$ satisfies*

$$(\mathbf{A} + \Delta\mathbf{A})\hat{\mathbf{x}} = \mathbf{b},$$

such that

$$|\Delta\mathbf{A}| \leq \tilde{\gamma}_{LS}|\hat{\mathbf{L}}||\hat{\mathbf{U}}|; \quad \tilde{\gamma}_{LS} \triangleq 2\tilde{\gamma}_1 + \tilde{\gamma}_2 + \tilde{\gamma}_1\tilde{\gamma}_2,$$

holds with a probability at least

$$\mathcal{T}_{LS}^b(\lambda, u, n) = 1 - [(1 - \mathcal{T}_{LU}^b) + (1 - \mathcal{T}_{FS}^b) + (1 - \mathcal{T}_{BS}^b)].$$

Proof. From [Lemma 4.2](#), the computed LU-factorization $\hat{\mathbf{L}}$ and $\hat{\mathbf{U}}$ satisfies $\hat{\mathbf{L}}\hat{\mathbf{U}} = (\mathbf{A} + \Delta\mathbf{A}')$ where component-wise $|\Delta\mathbf{A}'| \leq \tilde{\gamma}_1|\hat{\mathbf{L}}||\hat{\mathbf{U}}|$ holds with probability at least \mathcal{T}_{LU}^b . By [Lemma 4.3](#), forward substitution results in a computed solution $\hat{\mathbf{y}}$ which satisfies

$$(\hat{\mathbf{L}} + \Delta\hat{\mathbf{L}})\hat{\mathbf{y}} = \mathbf{b},$$

where component-wise $|\Delta\hat{\mathbf{L}}| \leq \tilde{\gamma}_1|\hat{\mathbf{L}}|$ is satisfied with probability at least \mathcal{T}_{FS}^b . For backward substitution, via [Lemma 4.4](#), the computed solution $\hat{\mathbf{x}}$ satisfies

$$(\hat{\mathbf{U}} + \Delta\hat{\mathbf{U}})\hat{\mathbf{x}} = \hat{\mathbf{y}},$$

where component-wise $|\Delta\hat{\mathbf{U}}| \leq \tilde{\gamma}_2|\hat{\mathbf{U}}|$ is satisfied with probability at least \mathcal{T}_{BS}^b . Thus,

$$\begin{aligned} (\hat{\mathbf{L}} + \Delta\hat{\mathbf{L}})(\hat{\mathbf{U}} + \Delta\hat{\mathbf{U}})\hat{\mathbf{x}} &= \mathbf{b}, \\ (\mathbf{A} + \Delta\mathbf{A})\hat{\mathbf{x}} &= \mathbf{b}, \end{aligned}$$

where $|\Delta \mathbf{A}| \leq (2\tilde{\gamma}_1 + \tilde{\gamma}_2 + \tilde{\gamma}_1\tilde{\gamma}_2)|\hat{\mathbf{L}}||\hat{\mathbf{U}}| = \tilde{\gamma}_{LS}|\hat{\mathbf{L}}||\hat{\mathbf{U}}|$ is satisfied with probability at least

$$\mathcal{T}_{LS}^b(\lambda, \mathbf{u}, n) = 1 - [(1 - \mathcal{T}_{LU}^b) + (1 - \mathcal{T}_{FS}^b) + (1 - \mathcal{T}_{BS}^b)].$$

□

Similarly, DBEA can be performed to obtain the backward error bounds as $|\Delta \mathbf{A}| \leq \gamma_{LS}|\hat{\mathbf{L}}||\hat{\mathbf{U}}|$ where $\gamma_{LS} \triangleq \gamma_1 + \gamma_2 + \gamma_1\gamma_2$. Performing MIBEA results in similar backward error bounds as [Theorem 4.5](#), however, the probability lower bound is $\mathcal{T}_{LS}^h(\lambda, \mathbf{u}, n) \triangleq 1 - [(1 - \mathcal{T}_{LU}^h) + (1 - \mathcal{T}_{FS}^h) + (1 - \mathcal{T}_{BS}^h)]$.

Using [Theorem 4.5](#), the corresponding probabilistic relative forward error bound is given as

$$(4.3) \quad \frac{\|\hat{\mathbf{x}} - \mathbf{x}\|_\infty}{\|\hat{\mathbf{x}}\|_\infty} \leq \tilde{\gamma}_{LS}\mathcal{C}_{LS}; \quad \mathcal{C}_{LS} \triangleq \frac{\|\mathbf{A}^{-1}(|\hat{\mathbf{L}}||\hat{\mathbf{U}}|\|\hat{\mathbf{x}}\|)\|_\infty}{\|\hat{\mathbf{x}}\|_\infty},$$

which holds with a probability at least \mathcal{T}_{LS}^b [[19](#), [Theorem 7.4](#)]. Similarly, for DBEA the relative forward error bound is $\gamma_{LS}\mathcal{C}_{LS}$, and for MIBEA it is given as $\tilde{\gamma}_{LS}\mathcal{C}_{LS}$ which holds with probability at least \mathcal{T}_{LS}^h .

5. Numerical Experiments. In this section, numerical experiments are presented. First, the variance-informed rounding uncertainty analysis is conducted for the dot product of random vectors. This is followed by a stochastic boundary-value problem with underlying uncertainties due to parameters, numerical discretization, sampling, and rounding. Such statistical models are widely used in practice wherein different sources of uncertainties must be quantified for optimal computational resource allocation while ensuring reliable model predictions.

5.1. Dot Product. Consider a dot product of random vectors $\mathbf{a}, \mathbf{b} \in \mathbb{F}^n$ given as $y = \mathbf{a}^T \mathbf{b}$. Numerically, this dot product is computed using the recursive relation $s_i = s_{i-1} + a_i b_i$ with $s_0 = 0$, such that $y = s_n$. Since the random vectors belong to the floating-point space, only rounding error due to operation is incurred, and therefore, the arithmetic model [\(2.4\)](#) is applicable. Theoretically, the backward error for the computed dot product \hat{y} is given as

$$(5.1) \quad \epsilon_{bwd} = \min\{\epsilon \geq 0 : \hat{y} = (\mathbf{a} + \Delta \mathbf{a})^T \mathbf{b}, |\Delta \mathbf{a}| \leq \epsilon |\mathbf{a}|\} = \frac{|\hat{y} - y|}{|\mathbf{a}^T \mathbf{b}|},$$

which is a random variable in the case where \mathbf{a} and \mathbf{b} are random vectors. To obtain the variance-informed backward error bounds, a critical λ -parameter can be defined as $\lambda_D^b(\alpha, \mathbf{u}, n) \triangleq \min\{\lambda \geq 0 : |\mathcal{T}_D^b(\lambda, \mathbf{u}, n) - \alpha|\}$, where $\alpha \in [0, 1]$ is the minimum required confidence for the backward bound to be satisfied. A large α would mean the backward error bound is satisfied with a larger probability. Similarly, for MIBEA we can define a critical λ -parameter as $\lambda_D^h(\alpha, \mathbf{u}, n) \triangleq \min\{\lambda \geq 0 : |\mathcal{T}_D^h(\lambda, \mathbf{u}, n) - \alpha|\}$. [Figure 6](#) illustrates the backward error and its bounds for dot product computed for random vectors distributed as $\mathcal{U}[-1, 1]$ and standard normal distribution. For the same confidence α , VIBEA results in tighter bounds than bounds obtained via DBEA and MIBEA.

[Figure 7](#) illustrates the empirical CDF for the relative forward error ϵ_{fwd}^{true} , and the modeled relative forward error ϵ_{fwd}^{model} (using [Model 2.1](#)) with its bounds. As observed, [Model 2.1](#) overestimates the accumulated error (lower CDF). As discussed in [§2.1](#), this overestimation is desirable as any bounds developed should not bound

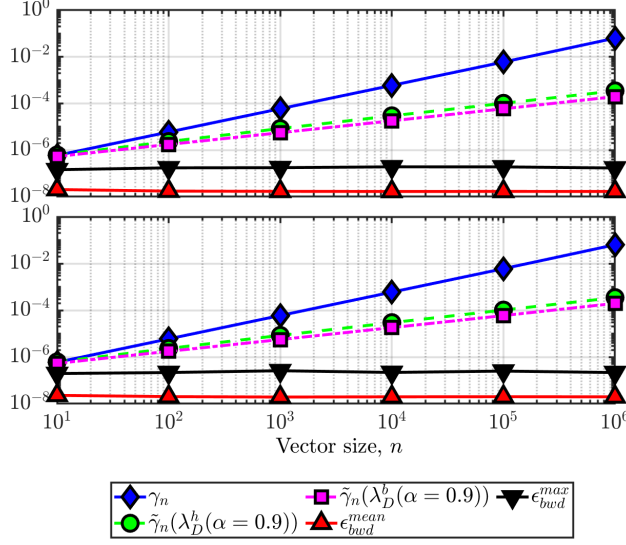


FIG. 6. Backward error and its bounds for the dot product of random vectors distributed as $\mathcal{U}[-1, 1]$ (top) and standard normal distribution (bottom) computed in fp32. To compute the statistics, 10^4 independent experiments are conducted.

an underpredicted accumulated rounding error. Like the backward error bounds, the variance-informed forward error bounds are tighter than those resulting from DBEA or MIBEA.

5.2. Boundary Value Problem. Consider the following boundary-value ODE with random coefficients and random forcing (adapted from [11])

$$(5.2) \quad \frac{d}{dx} \left((1 + \theta_1 x) \frac{du}{dx} \right) = -50\theta_2^2; \quad x \in [0, 1]; \quad u(0) = u(1) = 0,$$

where $\theta_1 \sim \mathcal{U}(0, 1) + 0.1$ and $\theta_2 \sim \mathcal{U}(0, 1) + 1$. The quantity of interest is $q = \mathbb{E}[P]$, where a realization of the variable P is given as $p(\theta_1, \theta_2) = \int_x u dx$. Numerically computing the quantity of interest is associated with multiple sources of uncertainty, namely, (a) parameter uncertainty, (b) numerical discretization, (c) Monte-Carlo integration, and (d) rounding.

5.2.1. Numerical discretizaion. For a given θ_1, θ_2 , (5.2) can be discretized via finite-difference method using M intervals of size $\Delta x \triangleq \frac{1}{M}$. Using second-order central difference approximation for the first- and second-order derivatives, the discretized form of the ODE is given as

$$(5.3) \quad \left(1 + \frac{\theta_1}{M} \left(i - \frac{1}{2}\right)\right) \tilde{u}_{i-1} - 2 \left(1 + \frac{\theta_1}{M} i\right) \tilde{u}_i + \left(1 + \frac{\theta_1}{M} \left(i + \frac{1}{2}\right)\right) \tilde{u}_{i+1} = -50\theta_2^2 \Delta x^2,$$

where \tilde{u}_i is the numerically approximated solution of $u(x)$ at $x = i\Delta x$ for $i = 1, \dots, M - 1$. This results in a tridiagonal system

$$(5.4) \quad \mathbf{A}(\theta_1) \tilde{\mathbf{u}} = \mathbf{b}(\theta_2),$$

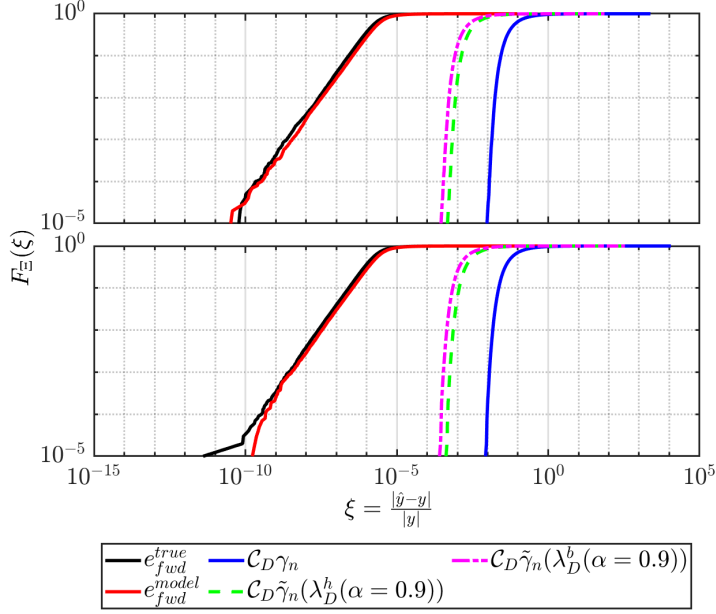


FIG. 7. Empirical CDF of relative forward error and its bounds for the dot product of random vectors distributed as $\mathcal{U}[-1, 1]$ (top) and standard normal distribution (bottom) computed in fp32. To compute the statistics, 10^5 independent experiments are conducted with vector size 10^4 .

where $\mathbf{A} \in \mathbb{R}^{(M-1) \times (M-1)}$, $\tilde{\mathbf{u}} \in \mathbb{R}^{(M-1)}$, $\mathbf{b} \in \mathbb{R}^{(M-1)}$. The non-zero elements of \mathbf{A} are given as

$$\begin{aligned} \mathbf{A}_{i,i-1} &\triangleq \alpha_i = 1 + \frac{\theta_1}{M} \left(i - \frac{1}{2}\right) & \text{for } i = 2, \dots, M-1, \\ \mathbf{A}_{i,i} &\triangleq \beta_i = -2 - 2\frac{\theta_1}{M} i & \text{for } i = 1, \dots, M-1, \\ \mathbf{A}_{i,i+1} &\triangleq \nu_i = 1 + \frac{\theta_1}{M} \left(i + \frac{1}{2}\right) & \text{for } i = 1, \dots, M-2. \end{aligned}$$

This system of equations can be solved via the Thomas algorithm to obtain the solution $\tilde{\mathbf{u}}$. Thereafter, an approximation of the integral quantity p given by \tilde{p} can be obtained via Reimann integration as $\tilde{p} = \sum_{i=1}^{M-1} \tilde{u}_i \Delta x$. The approximate quantity of interest \tilde{q} can then be obtained via Monte-Carlo integration.

5.2.2. Error due to numerical discretization. Solving the ODE in (5.2) via numerical discretization introduces errors due to (a) coarse discretization (small M) and (b) numerically approximating the spatial derivatives (Taylor series approximation). Herein, we present error bounds due to numerical discretization for a given finite-difference stencil.

For a given θ_1, θ_2 , consider $u(x) = f(x; \theta_1, \theta_2)$ as the ‘true’ solution to the ODE in (5.2), where $f(x; \theta_1, \theta_2)$ is assumed to be infinitely differentiable. Consider a restrictive operator $\mathcal{R} : \Omega \rightarrow \mathbb{R}^{M-1}$, which maps the true solution from the continuous domain Ω to the discrete space. The error due to numerical approximation is then

given as

$$\begin{aligned}\epsilon_d &\triangleq \mathcal{R}u - \tilde{\mathbf{u}}, \\ &= \mathbf{A}^{-1}\mathbf{A}\mathcal{R}u - \mathbf{A}^{-1}\mathbf{b}, \\ &= \mathbf{A}^{-1}(\mathbf{A}\mathcal{R}u - \mathbf{b}).\end{aligned}$$

For the discretized system in (5.3)

$$(\mathbf{A}\mathcal{R}u - \mathbf{b})_i \triangleq t_i = \alpha_i u_{i-1} + \beta_i u_i + \nu_i u_{i+1} + 50\theta_2^2 \Delta x^2,$$

where $u_i = u(x_i) = f(i\Delta x; \theta_1, \theta_2)$. Using Taylor-series expansion with the Lagrange remainder theorem to represent $u_{i\pm 1}$ gives

$$\begin{aligned}u(x_{i-1}) &= u(x_i) - \Delta x u'(x_i) + \frac{\Delta x^2}{2!} u''(x_i) - \frac{\Delta x^3}{3!} u'''(c_i^-), \\ u(x_{i+1}) &= u(x_i) + \Delta x u'(x_i) + \frac{\Delta x^2}{2!} u''(x_i) + \frac{\Delta x^3}{3!} u'''(c_i^+),\end{aligned}$$

for $c_i^- \in [x_{i-1}, x_i]$ and $c_i^+ \in [x_i, x_{i+1}]$. Since c_i^- and c_i^+ are unknown, we can bound $u(x_{i-1})$ and $u(x_{i+1})$ by defining

$$\begin{aligned}u_{i-1}^{\sup} &\triangleq \sup\{u(x_i) - \Delta x u'(x_i) + \frac{\Delta x^2}{2!} u''(x_i) - \frac{\Delta x^3}{3!} u'''(c_i^-)\}, \\ u_{i-1}^{\inf} &\triangleq \inf\{u(x_i) - \Delta x u'(x_i) + \frac{\Delta x^2}{2!} u''(x_i) - \frac{\Delta x^3}{3!} u'''(c_i^-)\}, \\ u_{i+1}^{\sup} &\triangleq \sup\{u(x_i) + \Delta x u'(x_i) + \frac{\Delta x^2}{2!} u''(x_i) + \frac{\Delta x^3}{3!} u'''(c_i^+)\}, \\ u_{i+1}^{\inf} &\triangleq \inf\{u(x_i) + \Delta x u'(x_i) + \frac{\Delta x^2}{2!} u''(x_i) + \frac{\Delta x^3}{3!} u'''(c_i^+)\},\end{aligned}$$

such that we can obtain the bounds for

(5.5a)

$$t_i^{\sup} \triangleq \sup\{\alpha_i * \ell_1 + \beta_i u_i + \nu_i \ell_2 + 50\theta_2^2 \Delta x^3 : \ell_1 \in [u_{i-1}^{\inf}, u_{i-1}^{\sup}], \ell_2 \in [u_{i+1}^{\inf}, u_{i+1}^{\sup}]\},$$

(5.5b)

$$t_i^{\inf} \triangleq \inf\{\alpha_i * \ell_1 + \beta_i u_i + \nu_i \ell_2 + 50\theta_2^2 \Delta x^3 : \ell_1 \in [u_{i-1}^{\inf}, u_{i-1}^{\sup}], \ell_2 \in [u_{i+1}^{\inf}, u_{i+1}^{\sup}]\},$$

which gives $\epsilon_d \in [\mathbf{A}^{-1}\mathbf{t}^{\sup}, \mathbf{A}^{-1}\mathbf{t}^{\inf}]$. The discretization error bounds are illustrated in Figure 8. Figure 9 illustrates the empirical CDF of the numerical discretization error and its bounds. As expected, refining the discretization reduces the error introduced due to numerical discretization. Further, the obtained bounds follow the same trend and can predict the numerical discretization error within an order of magnitude.

5.2.3. Error due to operation-rounding. Computing the integral quantity \bar{p} using finite-precision arithmetic results in several rounding errors due to operations. Broadly, such rounding errors accumulate when (a) solving the tri-diagonal system as described in §5.2.1, and (b) performing Reimann integration.

For the discretized system given in (5.4), the theoretical backward error is given as

$$(5.6) \quad \epsilon_{bwd} = \min\{\epsilon \geq 0 : (\mathbf{A} + \Delta\mathbf{A})\hat{\mathbf{u}} = \mathbf{b}, |\Delta\mathbf{A}| \leq \epsilon|\hat{\mathbf{L}}||\hat{\mathbf{U}}|\} = \max_i \frac{|\mathbf{A}\hat{\mathbf{u}} - \mathbf{b}|_i}{(|\hat{\mathbf{L}}||\hat{\mathbf{U}}||\hat{\mathbf{u}}|)_i},$$

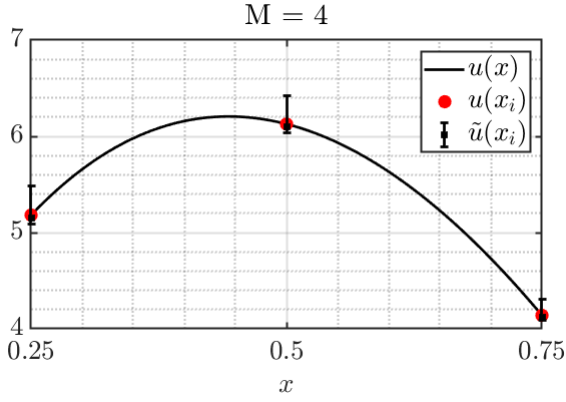


FIG. 8. Illustration of numerical discretization error bounds for $M = 4$.

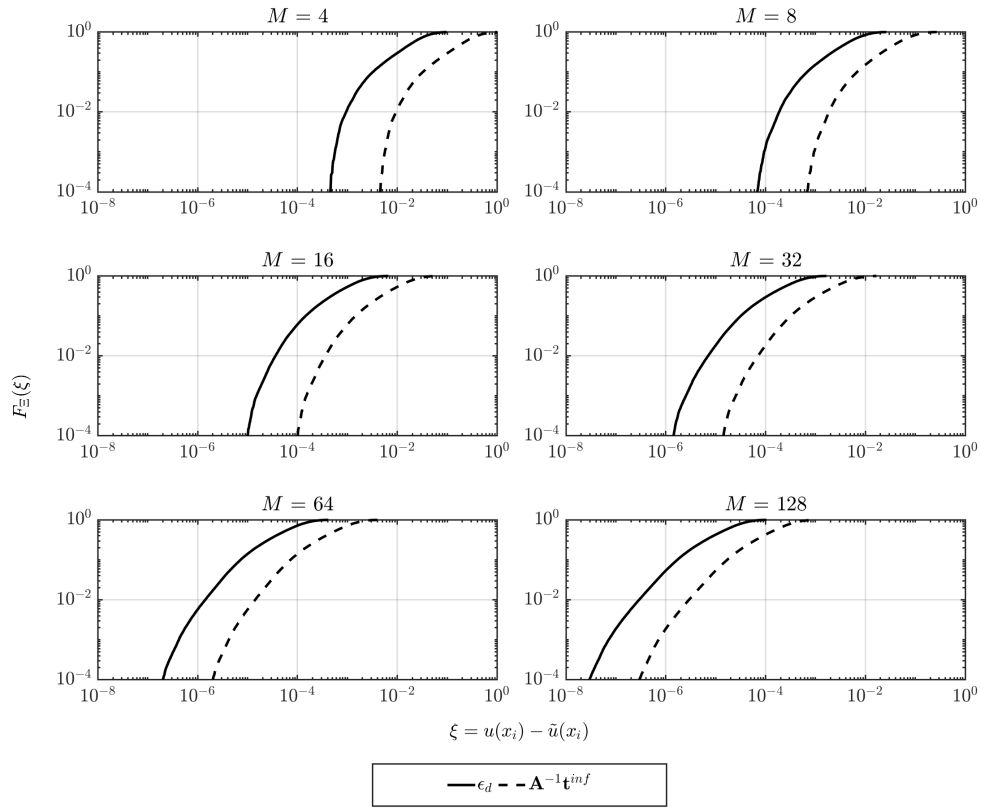


FIG. 9. Empirical CDF for discretization error and its bounds. 10^4 independent experiments are conducted to obtain the statistics. Solid line: true numerical discretization error; dashed line: upper bound for the numerical discretization error.

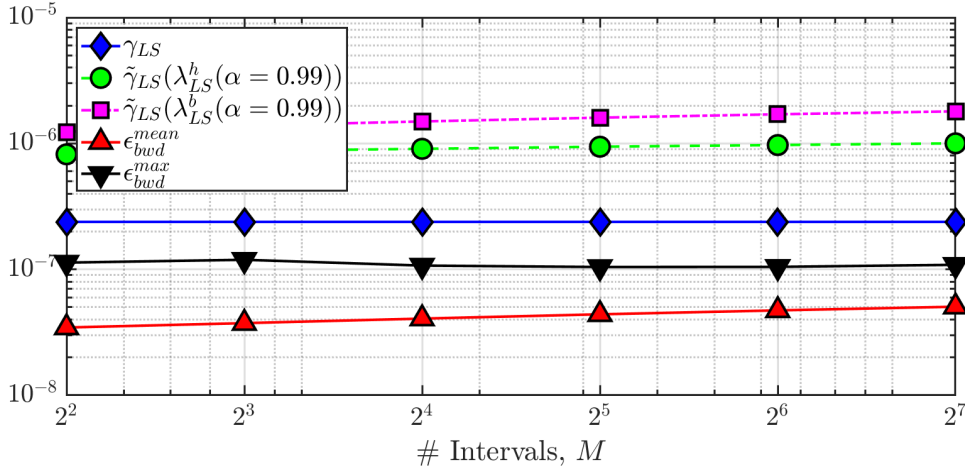


FIG. 10. Backward error and its bounds for ODE solution vs. number of discretization intervals m . Here, computations are performed in $fp32$, and 10^5 independent experiments are conducted to compute the statistics.

via Oettli-Prager theorem [19, Theorem 7.3]. Using Theorem 4.5, variance-informed backward error bounds for solving the tri-diagonal system can be obtained as

$$(5.7) \quad (\mathbf{A} + \Delta\mathbf{A})\hat{\mathbf{u}} = \mathbf{b}; \quad |\Delta\mathbf{A}| \leq \tilde{\gamma}_{LS}|\hat{\mathbf{L}}||\hat{\mathbf{U}}|,$$

which holds with probability at least $\mathcal{T}_{LS}^b(\lambda, \mathbf{u}, M-1)$ and $\mathcal{T}_{LS}^h(\lambda, \mathbf{u}, M-1)$ for VIBEA and MIBEA, respectively. The corresponding critical λ -parameter are defined as $\lambda_{LS}^b(\alpha, \mathbf{u}, M) \triangleq \min\{\lambda \geq 0 : |\mathcal{T}_{LS}^b(\lambda, \mathbf{u}, M-1) - \alpha|\}$ and $\lambda_{LS}^h(\alpha, \mathbf{u}, M) \triangleq \min\{\lambda \geq 0 : |\mathcal{T}_{LS}^h(\lambda, \mathbf{u}, M-1) - \alpha|\}$. Similarly, for DBEA the backward error bound is $\gamma_{LS}|\hat{\mathbf{L}}||\hat{\mathbf{U}}|$. Figure 10 illustrates the backward error and its bounds with varying discretization intervals. As observed, the deterministic treatment of rounding error (DBEA) results in tighter backward error bounds than the probabilistic treatment (VIBEA or MIBEA) across all the discretization intervals. This is due to the limited number of floating-point operations (at most 2 rounding error per floating-point number), which result in conservative probabilistic analysis, as discussed in §3. Further, as shown in Figure 5, for $n < 3$ and high confidence, VIBEA results in a larger critical λ -parameter and therefore is more conservative than MIBEA.

The absolute forward error bound for the discretized system (5.4) is given as

$$(5.8) \quad \|\hat{\mathbf{u}} - \tilde{\mathbf{u}}\|_\infty \leq \tilde{\gamma}_{LS}\mathcal{C}'_{LS}; \quad \mathcal{C}'_{LS} \triangleq \| |\mathbf{A}^{-1}|(|\hat{\mathbf{L}}||\hat{\mathbf{U}}||\hat{\mathbf{u}})|\|_\infty,$$

which also holds with probability at least $\mathcal{T}_{LS}^b(\lambda, \mathbf{u}, M-1)$ and $\mathcal{T}_{LS}^h(\lambda, \mathbf{u}, M-1)$ for VIBEA and MIBEA, respectively. Similarly, for DBEA, the absolute forward error bound is $\gamma_{LS}\mathcal{C}'_{LS}$. Figure 11 illustrates the empirical CDF of absolute forward error, its bounds, and the numerical discretization error. For all discretization intervals, Model 2.1 is a good approximation and slightly overestimates the true forward error. Similar to Figure 10, DBEA results in tighter bounds than VIBEA and MIBEA. For coarser discretization (small M), the error introduced due to rounding is significantly lower. However, for large M , the number of finite-precision operations

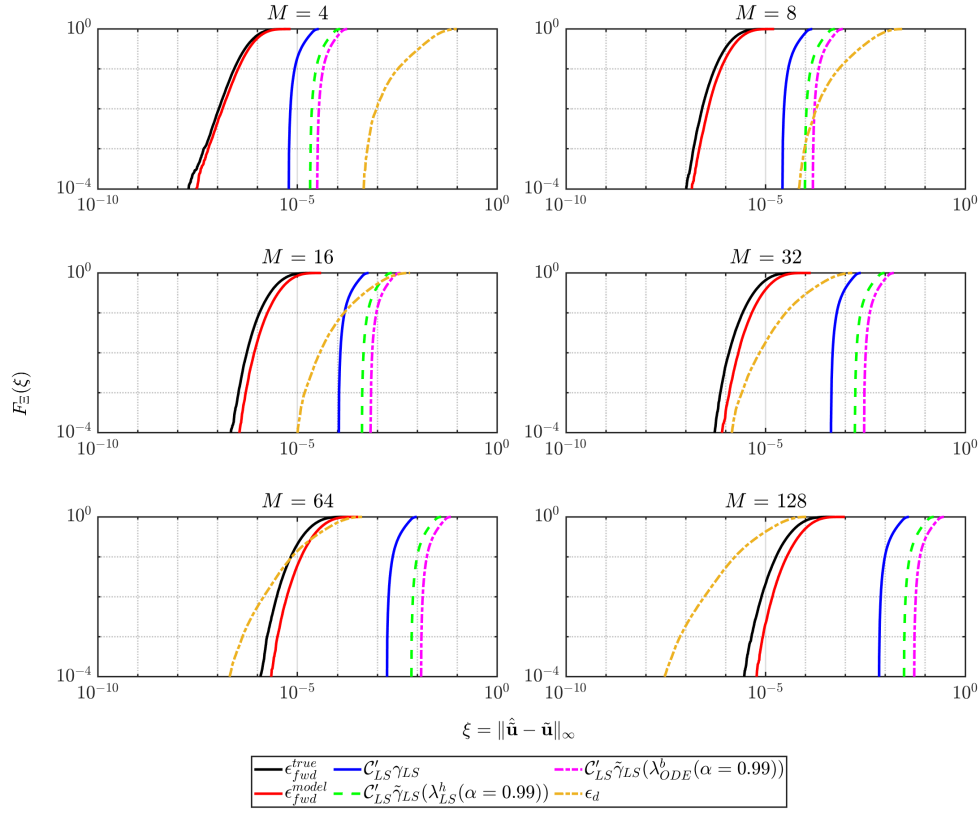


FIG. 11. Empirical CDF of the absolute forward error for ODE solution and its bounds along with numerical discretization error for the ODE solution computed in fp32. Here, 10^5 independent experiments are conducted to compute the statistics.

increases thereby increasing the error introduced due to rounding. For the computed solution $\hat{\mathbf{u}}$, Theorem 4.1 can then be used to compute the backward error bounds for the computed approximation \hat{p} of \tilde{p}

$$\hat{p} = \sum_{i=1}^{M-1} (\hat{u}_i + \Delta \hat{u}_i) \Delta x_i; \quad |\Delta \hat{u}_i| \leq \tilde{\gamma}_{M-1} |\hat{u}_i|,$$

which is satisfied with the probability of at least $\mathcal{T}_D^b(\lambda, u, M-1)$ and $\mathcal{T}_D^b(\lambda, u, M-1)$ for VIBEA and MIBEA, respectively. In the case of uniform grid spacing $\Delta x_i = \Delta x$. In addition to rounding error due to operation in performing the Riemann summation, there exists rounding error in computing $\hat{\mathbf{u}}$ as described by (5.8). Thus, the forward error in computing $\hat{\mathbf{u}}$ can be propagated to obtain the absolute error in performing

the Reimann integration as

$$\begin{aligned}
|\hat{p} - \tilde{p}| &= \left| \sum_{i=1}^{M-1} (\hat{u}_i - \tilde{u}_i) \Delta x + \Delta \hat{u}_i \Delta x \right|, \\
&\leq \sum_{i=1}^{M-1} |\hat{u}_i - \tilde{u}_i| |\Delta x| + |\Delta \hat{u}_i| |\Delta x|, \\
(5.9) \quad &\leq \Delta x \left((M-1) \tilde{\gamma}_{LS} \mathcal{C}'_{LS} + \tilde{\gamma}_{M-1} \|\hat{\mathbf{u}}\|_1 \right) \triangleq \tilde{\mathcal{J}},
\end{aligned}$$

which is satisfied with a probability of at least

$$(5.10) \quad \mathcal{T}_{ODE}^b(\lambda, \mathbf{u}, M) = 1 - \left[(1 - \mathcal{T}_D^b(\lambda, \mathbf{u}, M-1)) + (1 - \mathcal{T}_{LS}^b(\lambda, \mathbf{u}, M-1)) \right],$$

and

$$(5.11) \quad \mathcal{T}_{ODE}^h(\lambda, \mathbf{u}, M) = 1 - \left[(1 - \mathcal{T}_D^h(\lambda, \mathbf{u}, M-1)) + (1 - \mathcal{T}_{LS}^h(\lambda, \mathbf{u}, M-1)) \right],$$

for VIBEA and MIBEA, respectively. To compare the obtained probabilistic bounds, critical λ -parameter can then be defined as $\lambda_{ODE}^b \triangleq \min\{\lambda \geq 0 : |\mathcal{T}_{ODE}^b - \alpha|\}$ and $\lambda_{ODE}^h \triangleq \min\{\lambda \geq 0 : |\mathcal{T}_{ODE}^h - \alpha|\}$. Following a similar approach, the absolute forward error bound obtained via DBEA is given as $\mathcal{J} \triangleq \Delta x \left((M-1) \gamma_{LS} \mathcal{C}'_{LS} + \gamma_{M-1} \|\hat{\mathbf{u}}\|_1 \right)$. [Figure 12](#) shows the empirical CDF for the absolute forward error in computing \tilde{p} and its bounds. A similar trend is observed for the error bounds for computing \tilde{p} as observed for $\tilde{\mathbf{u}}$. [Figure 13](#) illustrates the absolute errors in Monte-Carlo integration for $\mathbb{E}[P]$, using analytical and numerical evaluation. For small M , errors remain consistent across precisions, indicating dominant uncertainty from numerical discretization over rounding or sampling. At $M \in \{16, 32, 64\}$, half-precision yields comparable errors to analytical or higher precisions, improving as n increases, reducing sampling uncertainty. However, at $M = 128$, the accumulated rounding error is significantly higher compared to the numerical discretization error (maximum discretization error is $\mathcal{O}(u_{half})$). Thus, higher precision is required for reliable model prediction at finer discretization.

6. Concluding Remarks and Perspectives. We present a novel variance-informed probabilistic backward error analysis, called VIBEA, for quantifying the uncertainty arising from rounding errors in floating-point computations. The probabilistic bounds assume that the rounding errors due to representation- or operation-rounding are i.i.d. random variables distributed uniformly as $\mathcal{U}[-u, u]$. The goal is to estimate rounding uncertainty by exploiting the statistical effect introduced due to the probabilistic description of rounding errors. We assume the standard IEEE arithmetic model, which introduces terms of the form $\phi = \prod_{i=1}^n (1 + \delta_i)$ where δ_i represents the rounding errors. Nevertheless, it is important to acknowledge that the widely adopted IEEE arithmetic model does not encompass all rounding artifacts. For example, rounding errors are not enforced to be identically zero when the computed value belongs to the floating-point system. The rationale behind its usage is deriving an *average* rounding uncertainty estimate stemming from the statistical implications of the probabilistic assumption regarding rounding errors. We utilize concentration inequalities that exploit high-order rounding error statistics to obtain probabilistic rounding uncertainty estimates. Specifically, we utilize Bernstein's concentration inequality to develop probabilistic bounds for $\log \phi$.

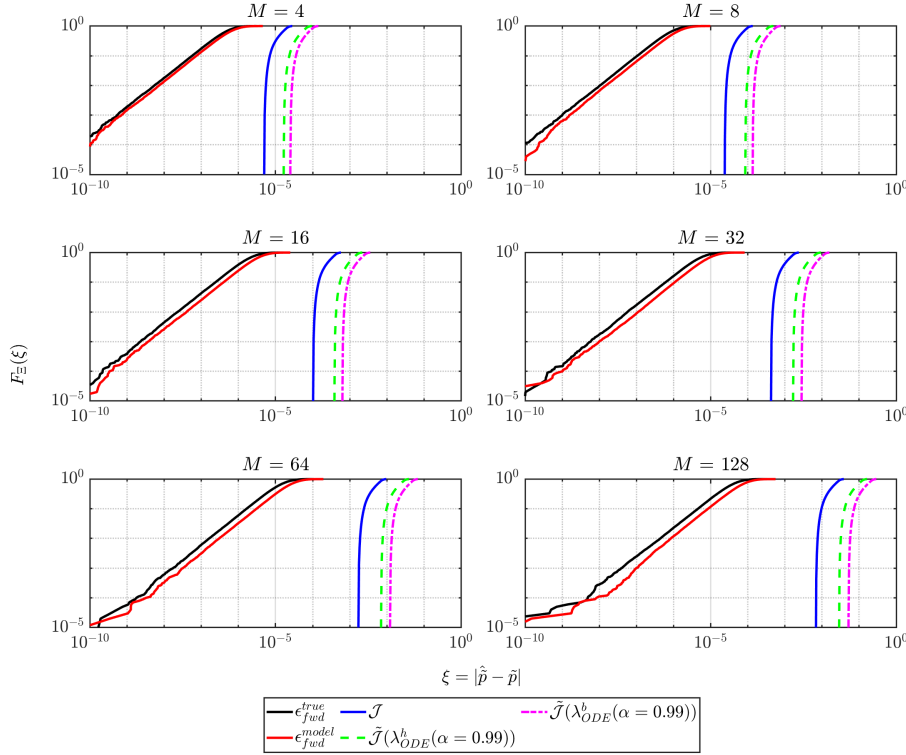


FIG. 12. Empirical CDF of absolute forward error and its bounds for the integral quantity of interest \tilde{p} computed in fp32.

We show that the i.i.d. assumption results in a marginal overestimation of the true accumulated rounding error for all the cases, suggesting its candidacy as a valid model for developing probabilistic rounding error bounds. Compared to the traditional deterministic analysis that involves the constant $\gamma_n = nu/(1-nu)$, the proposed backward error analysis replaces γ_n with $\tilde{\gamma}_n = \lambda\sqrt{nu}$ such that the resulting rounding error bounds grow slowly with problem size n . We show that for $n > 50$, high confidence error bounds can be obtained via VIBEA compared to the deterministic analysis. By introducing higher-order statistics of the rounding error, we show that the resulting bounds are tighter than those obtained by the mean-informed rounding uncertainty analysis (called MIBEA in this work) recently presented by Higham and Mary [20]. Specifically, we show that VIBEA can result in high confidence bounds for $n \geq 3$ compared to the mean-informed probabilistic analysis.

Backward and forward error bounds are derived for the dot product of vectors and solving a tri-diagonal system via Thomas' algorithm. Numerical experiments performed for the dot product of random vectors illustrate that VIBEA results in tighter backward and forward error bounds compared to the deterministic analysis and MIBEA. We also explored a stochastic boundary value problem with intrinsic uncertainties arising from varied sources such as parameters, sampling, numerical discretization, and rounding. A probabilistic approach towards backward-forward error analysis is introduced, which accurately estimates the uncertainty introduced due to rounding. We acknowledge that our assumption that representation and operation

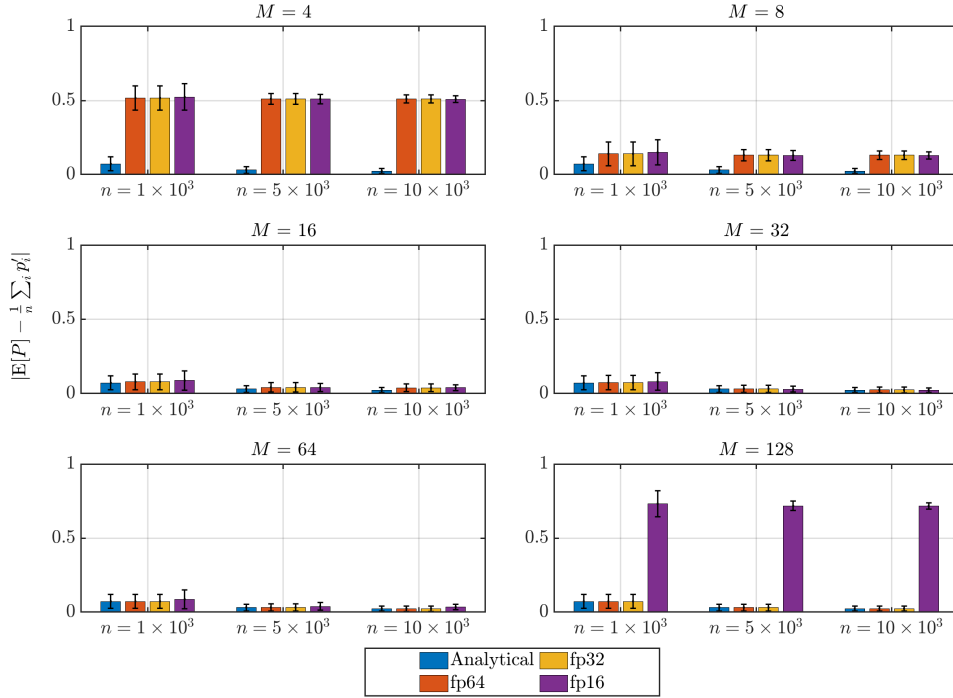


FIG. 13. Absolute forward error in computing the quantity of interest $\mathbb{E}[P]$ via Monte-Carlo integration. Here, $p' = p$ for analytical, and $p' = \tilde{p}$ is the numerical evaluation using the respective precision.

rounding errors are both i.i.d. uniform random variables is a simplistic model and may not always be valid, such as when performing integer arithmetic where rounding errors are identically zero, nevertheless we obtain useful results. Error bounds are presented for quantifying uncertainty due to numerical discretization and are shown to be accurate within an order of magnitude.

In most of the presented examples, we show that the uncertainty introduced due to low precision is small relative to that by numerical discretization or sampling. Therefore, reliable model predictions can be obtained with low-precision arithmetic at coarser discretization without allocating computational efforts to reduce sampling uncertainty. However, as the uncertainty due to numerical discretization diminishes, the uncertainty due to rounding becomes more prominent.

This work highlights the need to understand the different uncertainties in floating-point statistical models for more nuanced optimization strategies, such as balancing numerical discretization with evaluation precision or the requisite parameter samples for addressing sampling uncertainty. The insights from such a comprehensive uncertainty budgeting are crucial for strategically allocating computational efforts, enabling the development of reliable and cost-efficient models.

Reproducibility of Computational Results. Code for the experiments performed in this article is available at <https://github.com/sahilbhola14/FinUQ>.

Acknowledgments. This work is dedicated to the memory of the late Prof. Nick Higham whose work continues to inspire the field of numerical analysis. We thank

Profs. Jean-Baptiste Jeannin and Alex Gorodetsky for advice and for the valuable feedback on the early drafts of this manuscript. This research was supported by NSF Grant FMITF-2219997.

REFERENCES

- [1] NVIDIA Blackwell architecture reference manual. <https://resources.nvidia.com/en-us-blackwell-architecture>.
- [2] A. ABDELFATTAH, H. ANZT, E. G. BOMAN, E. CARSON, T. COJEAN, J. DONGARRA, A. FOX, M. GATES, N. J. HIGHAM, X. S. LI, ET AL., *A survey of numerical linear algebra methods utilizing mixed-precision arithmetic*, The International Journal of High Performance Computing Applications, 35 (2021), pp. 344–369.
- [3] M. BABOULIN, A. BUTTARI, J. DONGARRA, J. KURZAK, J. LANGOU, J. LANGOU, P. LUSZCZEK, AND S. TOMOV, *Accelerating scientific computations with mixed precision algorithms*, Computer Physics Communications, 180 (2009), pp. 2526–2533.
- [4] S. BOUCHERON, G. LUGOSI, AND O. BOUSQUET, *Concentration inequalities*, in Summer school on machine learning, Springer, 2003, pp. 208–240.
- [5] A. BUTTARI, J. DONGARRA, J. LANGOU, J. LANGOU, P. LUSZCZEK, AND J. KURZAK, *Mixed precision iterative refinement techniques for the solution of dense linear systems*, The International Journal of High Performance Computing Applications, 21 (2007), pp. 457–466.
- [6] A. BUTTARI, N. J. HIGHAM, T. MARY, AND B. VIEUBLÉ, *A modular framework for the backward error analysis of gmres*, (2024).
- [7] A. CHEREZOV, A. VASILIEV, AND H. FERROUKHI, *Acceleration of nuclear reactor simulation and uncertainty quantification using low-precision arithmetic*, Applied Sciences, 13 (2023), p. 896.
- [8] M. P. CONNOLLY AND N. J. HIGHAM, *Probabilistic rounding error analysis of householder qr factorization*, SIAM Journal on Matrix Analysis and Applications, 44 (2023), pp. 1146–1163.
- [9] M. CROCI, M. FASI, N. J. HIGHAM, T. MARY, AND M. MIKAITIS, *Stochastic rounding: implementation, error analysis and applications*, Royal Society Open Science, 9 (2022), p. 211631.
- [10] B. FENG, Y. WANG, G. CHEN, W. ZHANG, Y. XIE, AND Y. DING, *Egemm-tc: accelerating scientific computing on tensor cores with extended precision*, in Proceedings of the 26th ACM SIGPLAN symposium on principles and practice of parallel programming, 2021, pp. 278–291.
- [11] M. B. GILES, *Multilevel monte carlo methods*, Acta numerica, 24 (2015), pp. 259–328.
- [12] S. GUPTA, A. AGRAWAL, K. GOPALAKRISHNAN, AND P. NARAYANAN, *Deep learning with limited numerical precision*, in International conference on machine learning, PMLR, 2015, pp. 1737–1746.
- [13] A. HAIDAR, H. BAYRAKTAR, S. TOMOV, J. DONGARRA, AND N. J. HIGHAM, *Mixed-precision iterative refinement using tensor cores on gpus to accelerate solution of linear systems*, Proceedings of the Royal Society A, 476 (2020), p. 20200110.
- [14] A. HAIDAR, P. WU, S. TOMOV, AND J. DONGARRA, *Investigating half precision arithmetic to accelerate dense linear system solvers*, in Proceedings of the 8th workshop on latest advances in scalable algorithms for large-scale systems, 2017, pp. 1–8.
- [15] S. HATFIELD, M. CHANTRY, P. DÜBEN, AND T. PALMER, *Accelerating high-resolution weather models with deep-learning hardware*, in Proceedings of the platform for advanced scientific computing conference, 2019, pp. 1–11.
- [16] P. HENRICI, *Test of probabilistic models for the propagation of roundoff errors*, Communications of the ACM, 9 (1966), pp. 409–410.
- [17] N. J. HIGHAM, *How accurate is gaussian elimination?*, tech. report, Cornell University, 1989.
- [18] N. J. HIGHAM, *Bounding the error in gaussian elimination for tridiagonal systems*, SIAM journal on matrix analysis and applications, 11 (1990), pp. 521–530.
- [19] N. J. HIGHAM, *Accuracy and stability of numerical algorithms*, SIAM, 2002.
- [20] N. J. HIGHAM AND T. MARY, *A new approach to probabilistic rounding error analysis*, SIAM journal on scientific computing, 41 (2019), pp. A2815–A2835.
- [21] N. J. HIGHAM AND T. MARY, *Sharper probabilistic backward error analysis for basic linear algebra kernels with random data*, SIAM Journal on Scientific Computing, 42 (2020), pp. A3427–A3446.
- [22] N. J. HIGHAM AND S. PRANESH, *Simulating low precision floating-point arithmetic, mims eprint*

- 2019.4, Manchester Institute for Mathematical Sciences, The University of Manchester, UK, (2019).
- [23] N. J. HIGHAM, S. PRANESH, AND M. ZOUNON, *Squeezing a matrix into half precision, with an application to solving linear systems*, SIAM journal on scientific computing, 41 (2019), pp. A2536–A2551.
 - [24] I. HUBARA, M. COURBARIAUX, D. SOUDRY, R. EL-YANIV, AND Y. BENGIO, *Quantized neural networks: Training neural networks with low precision weights and activations*, Journal of Machine Learning Research, 18 (2018), pp. 1–30.
 - [25] T. E. HULL AND J. R. SWENSON, *Tests of probabilistic models for propagation of roundoff errors*, Communications of the ACM, 9 (1966), pp. 108–113.
 - [26] IEEE, *Ieee standard for floating-point arithmetic, ieee std 754-2019 (revision of ieee 754-2008)*, Institute of Electrical and Electronics Engineers New York, 2019.
 - [27] I. C. IPSEN AND H. ZHOU, *Probabilistic error analysis for inner products*, SIAM journal on matrix analysis and applications, 41 (2020), pp. 1726–1741.
 - [28] M. KARP, F. LIU, R. STANLY, S. REZAEIRAVESH, N. JANSSON, P. SCHLATTER, AND S. MARKIDIS, *Uncertainty quantification of reduced-precision time series in turbulent channel flow*, in Proceedings of the SC’23 Workshops of The International Conference on High Performance Computing, Network, Storage, and Analysis, 2023, pp. 387–390.
 - [29] A. E. KELLISON, A. W. APPEL, M. TEKRIWAL, AND D. BINDEL, *Laproof: A library of formal proofs of accuracy and correctness for linear algebra programs*, in Proceedings of the 30th IEEE International Symposium on Computer Arithmetic (ARITH)(Sept. 2023). <https://github.com/ak-2485/ak-2485.github.io/blob/master/laproof.pdf>, 2023.
 - [30] T. KIMPSON, E. A. PAXTON, M. CHANTRY, AND T. PALMER, *Climate-change modelling at reduced floating-point precision with stochastic rounding*, Quarterly Journal of the Royal Meteorological Society, 149 (2023), pp. 843–855.
 - [31] G. LIENHART, A. KUGEL, AND R. MANNER, *Using floating-point arithmetic on fpgas to accelerate scientific n-body simulations*, in Proceedings. 10th Annual IEEE Symposium on Field-Programmable Custom Computing Machines, IEEE, 2002, pp. 182–191.
 - [32] Y. LIU, X. LIU, AND E. WU, *Real-time 3d fluid simulation on gpu with complex obstacles*, in 12th Pacific Conference on Computer Graphics and Applications, 2004. PG 2004. Proceedings., IEEE, 2004, pp. 247–256.
 - [33] S. MITTAL, *A survey of techniques for approximate computing*, ACM Computing Surveys (CSUR), 48 (2016), pp. 1–33.
 - [34] D. MORI, Y. YAMAMOTO, AND S.-L. ZHANG, *Backward error analysis of the allreduce algorithm for householder qr decomposition*, Japan journal of industrial and applied mathematics, 29 (2012), pp. 111–130.
 - [35] E. A. PAXTON, M. CHANTRY, M. KLÖWER, L. SAFFIN, AND T. PALMER, *Climate modeling in low precision: Effects of both deterministic and stochastic rounding*, Journal of Climate, 35 (2022), pp. 1215–1229.
 - [36] J. RICHARD SHEWCHUK, *Adaptive precision floating-point arithmetic and fast robust geometric predicates*, Discrete & Computational Geometry, 18 (1997), pp. 305–363.
 - [37] P. R. RINALDI, E. DARI, M. J. VÉNERE, AND A. CLAUSSE, *A lattice-boltzmann solver for 3d fluid simulation on gpu*, Simulation Modelling Practice and Theory, 25 (2012), pp. 163–171.
 - [38] C. J. ROY AND W. L. OBERKAMPF, *A comprehensive framework for verification, validation, and uncertainty quantification in scientific computing*, Computer methods in applied mechanics and engineering, 200 (2011), pp. 2131–2144.
 - [39] M. TIENARI, *A statistical model of roundoff error for varying length floating-point arithmetic*, BIT Numerical Mathematics, 10 (1970), pp. 355–365.
 - [40] J. VON NEUMANN AND H. H. GOLDSTINE, *Numerical inverting of matrices of high order*, (1947).
 - [41] S. WAN, R. C. SINCLAIR, AND P. V. COVENEY, *Uncertainty quantification in classical molecular dynamics*, Philosophical Transactions of the Royal Society A, 379 (2021), p. 20200082.
 - [42] N. WANG, J. CHOI, D. BRAND, C.-Y. CHEN, AND K. GOPALAKRISHNAN, *Training deep neural networks with 8-bit floating point numbers*, Advances in neural information processing systems, 31 (2018).
 - [43] J. H. WILKINSON, *Error analysis of direct methods of matrix inversion*, Journal of the ACM (JACM), 8 (1961), pp. 281–330.
 - [44] J. H. WILKINSON, *Rounding errors in algebraic processes*, SIAM, 2023.